LETTERS

Broken rotational symmetry in the pseudogap phase of a high-T_c superconductor

R. Daou[1]†, J. Chang[1], David LeBoeuf[1], Olivier Cyr-Choinière[1], Francis Laliberté[1], Nicolas Doiron-Leyraud[1], B. J. Ramshaw[2], Ruixing Liang[2,3], D. A. Bonn[2,3], W. N. Hardy[2,3] & Louis Taillefer[1,3]

The nature of the pseudogap phase is a central problem in the effort to understand the high-transition-temperature (high-T_c) copper oxide superconductors[1]. A fundamental question is what symmetries are broken when the pseudogap phase sets in, which occurs when the temperature decreases below a value T^*. There is evidence from measurements of both polarized neutron diffraction[2,3] and the polar Kerr effect[4] that time-reversal symmetry is broken, but at temperatures that differ significantly from one another. Broken rotational symmetry was detected from both resistivity measurements[5] and inelastic neutron scattering[6–8] at low doping, and from scanning tunnelling spectroscopy[9,10] at low temperature, but showed no clear relation to T^*. Here we report the observation of a large in-plane anisotropy of the Nernst effect in $YBa_2Cu_3O_y$ that sets in precisely at T^* throughout the doping phase diagram. We show that the CuO chains of the orthorhombic lattice are not responsible for this anisotropy, which is therefore an intrinsic property of the CuO_2 planes. We conclude that the pseudogap phase is an electronic state that strongly breaks four-fold rotational symmetry. This narrows the range of possible states considerably, pointing to stripe or nematic order[11,12].

We have measured the Nernst coefficient, $\nu(T)$, of the high-T_c superconductor $YBa_2Cu_3O_y$ (YBCO) as a function of temperature up to ~300 K for a hole concentration[13] (doping) ranging from $p = 0.08$ to $p = 0.18$, in untwinned crystals where the temperature gradient, ΔT, was applied along either the a axis or the b axis of the orthorhombic plane. Figure 1 shows a typical data set, which consists of two contributions: a positive, strongly field-dependent contribution due to superconducting fluctuations[14–16] and a field-independent contribution due to normal-state quasiparticles[17]. The second contribution changes from being small and positive to being large and negative as the temperature decreases. We define as T_ν the temperature at which ν/T begins to decrease. In Fig. 2, we plot T_ν as a function of doping. We also plot T_ρ, the temperature below which the in-plane resistivity, $\rho(T)$, of YBCO deviates negatively from its linear temperature dependence at high temperature, which is a standard definition of the pseudogap temperature, T^* (refs 18, 19). We see that $T_\nu = T_\rho$, within the errors, as also found in a recent study of YBCO films[20]. We also see that the value of T_ν obtained with ΔT parallel to the a axis ($\Delta T || a$) is the same as the value obtained with $\Delta T || b$, within the errors. We therefore conclude that the decrease in the quasiparticle Nernst signal to large negative values is a signature of the pseudogap phase, detectable up to the highest doping that we measured, $p = 0.18$.

In Fig. 3, we see that the dip in ν/T between T_ν and T_c gets shallower as the difference between T_ν and T_c shrinks with doping (Fig. 2). This characteristic dip is extremely anisotropic, being roughly ten times deeper when $\Delta T || b$ than when $\Delta T || a$. In Supplementary Fig. 6, we plot the Nernst anisotropy as a ratio, which is seen to reach $\nu_b/\nu_a \approx 7$ at 90 K for $p = 0.12$. To our knowledge, this is the largest in-plane anisotropy reported in any macroscopic physical property of any high-T_c superconductor[12]. In Fig. 4a, we plot the anisotropy difference $D(T) \equiv (\nu_a - \nu_b)/T$ relative to its value at T_ν, which reveals that the onset of the a–b anisotropy coincides with T_ν. This shows that the anisotropy is a property of the pseudogap phase, as $T_\nu = T^*$. In Fig. 4b, we plot the anisotropy difference divided by the sum $S(T) \equiv -(\nu_a + \nu_b)/T$, as $[D(T) - D(T_\nu)]/[S(T) - S(T_\nu)]$ versus T.

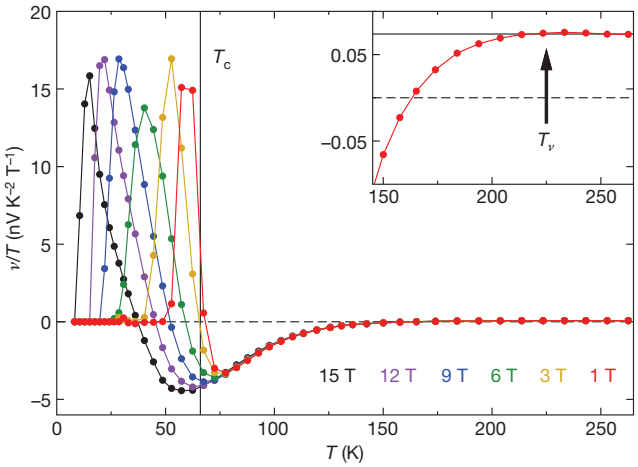

Figure 1 | Nernst coefficient. Nernst coefficient, ν, of YBCO, plotted as ν/T versus T, for different values of the magnetic field B (as colour-coded). The sample is a single crystal with an oxygen content of $y = 6.67$ and a superconducting transition temperature of $T_c(B = 0) = 66.0$ K (vertical line), corresponding to a hole concentration (doping) of $p = 0.12$ (ref. 13). The thermal gradient is along the b axis of the orthorhombic structure, the transverse Nernst voltage is measured along the a axis and the magnetic field is applied along the c axis. We see that $\nu(T)$ consists of two contributions: a field-independent contribution, attributed to quasiparticles, which is small and positive at high temperature and becomes large and negative on cooling; and a positive, strongly field-dependent contribution, attributed to superconducting fluctuations, which causes ν to rise sharply as the temperature approaches T_c from above. Inset, magnified view at high temperature, showing where ν/T starts to decrease below its constant, small and positive high-T value, at the onset temperature T_ν (arrow). The data for all samples are shown in the Supplementary Information (Supplementary Figs 1, 2 and 3) and the values of T_ν are listed in Supplementary Table 1. Our data are consistent with published YBCO data[14–16] wherever they overlap (in temperature and doping). In particular, a negative quasiparticle contribution has been observed for $p \approx 0.1$–0.15, in measurements mostly done on twinned crystals[14–16].

[1]Département de Physique and RQMP, Université de Sherbrooke, Sherbrooke, Québec J1K 2R1, Canada. [2]Department of Physics and Astronomy, University of British Columbia, Vancouver, British Columbia V6T 1Z1, Canada. [3]Canadian Institute for Advanced Research, Toronto, Ontario M5G 1Z8, Canada. †Present address: Max Planck Institute for Chemical Physics of Solids, 01187 Dresden, Germany.

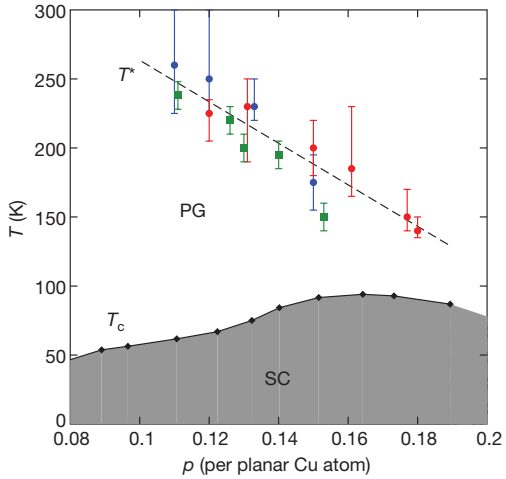

Figure 2 | Phase diagram. Temperature–doping phase diagram of YBCO showing the superconducting phase (SC) below the transition temperature, T_c (diamonds; from ref. 13). Two characteristic temperatures are plotted: T_ν (blue circles, $\Delta T \,||\, a$; red circles, $\Delta T \,||\, b$), which marks the onset of the decrease in the quasiparticle Nernst signal, as defined in Fig. 1 (see also Supplementary Figs 1 and 2); and T_ρ (green squares), which marks the onset of the decrease in the resistivity, $\rho(T)$, from its linear temperature dependence at high temperature, as defined in Supplementary Fig. 4 (using data from ref. 19). This definition of T_ρ is a standard definition of the pseudogap-phase (PG) onset temperature, T^*, in YBCO (ref. 18). The error bars on T_ν and T_ρ indicate the uncertainty in locating the temperature below which ν/T and $\rho(T)$ start to deviate from their respective behaviours at high temperature (Supplementary Information). The dashed line is a guide to the eye. Within the errors, we find that $T_\nu = T_\rho$, showing that the decrease in ν/T signals the onset of the pseudogap phase. We note that in ν_b/T (where ν_b is the Nernst coefficient measured with $\Delta T \,||\, b$), this signature remains clearly visible up to the highest doping that we measure ($p = 0.18$; Supplementary Fig. 1f), whereas it is not detectable in ν_a/T (ν_a measured with $\Delta T \,||\, a$) or ρ for dopings greater than $p \approx 0.15$ (Supplementary Fig. 2).

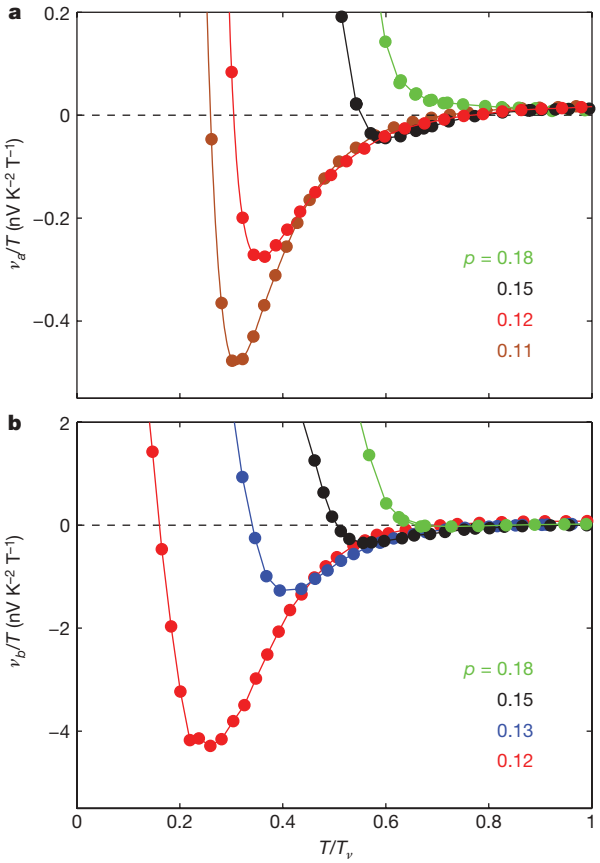

Figure 3 | Comparison of ν_a and ν_b. **a**, **b**, Dependence of ν/T on the normalized temperature T/T_ν for various dopings (as colour-coded), for $\Delta T \,||\, a$ (**a**) and $\Delta T \,||\, b$ (**b**). The T_ν values are those listed in Supplementary Table 1 and plotted in Fig. 2. Note that the vertical range is ten times larger in **b** than in **a**, showing that the negative quasiparticle Nernst signal is an order of magnitude larger for $\Delta T \,||\, b$.

The relative anisotropy, $D(T)/S(T) = (\nu_b - \nu_a)/(\nu_b + \nu_a)$, can be viewed as a Nernst-derived nematic-order parameter, in analogy with that defined from the resistivity[21].

In the orthorhombic crystal structure of YBCO, there are CuO chains along the b axis, between the CuO_2 planes common to all copper oxides. These chains can conduct charge, causing an anisotropy in the conductivity, σ, such that $\sigma_b/\sigma_a > 1$ (where σ_a and σ_b are the conductivities measured along the a and b axes, respectively). In principle, these chains could also cause an anisotropy in ν, but the chains in fact make a negligible contribution to ν. To see this, we first consider the low doping regime at $p = 0.08$ ($y = 6.45$), for which the anisotropy ratios of both σ and ν are displayed in Supplementary Fig. 6a. As established previously[5], the conductivity of chains decreases as p decreases, becoming negligible for $p \approx 0.08$, as shown by the fact that $\sigma_b/\sigma_a \approx 1$ at high temperature. Under conditions of negligible chain conduction, we observe a small increase in σ_b/σ_a as the temperature decreases (Supplementary Fig. 6a), which is convincing evidence of a state that breaks rotational symmetry, as previously reported[5]. The similar (but larger) increase in ν_b/ν_a (Supplementary Fig. 6a) is equivalent evidence of the same symmetry breaking. By contrast, at higher doping, such as $p = 0.12$ (Supplementary Fig. 6b), σ_b/σ_a decreases on cooling, which is the signature of chain-dominated conductivity[5]; the Nernst anisotropy, however, exhibits the same characteristic increase on cooling that it does for $p = 0.08$. This shows that although chains dominate the anisotropy in σ at higher doping, they appear to have little impact on the anisotropy in ν.

This is confirmed by a second test, where we greatly enhance the conductivity of the chains while keeping the doping approximately constant. This is done by comparing samples with $y = 6.97$ ($p = 0.177$) with samples with $y = 6.998$ ($p = 0.180$). Because the densities of oxygen vacancies in the chains are 3% and 0.2%, respectively, the chain conductivity of the samples with $y = 6.998$ is much larger, by a factor of four (Supplementary Fig. 8), than that of the other samples. The effect of this enhanced chain conductivity on the Nernst signal can be seen in the anisotropy difference, $D(T)$, plotted in Supplementary Fig. 9b. For $T > T_\nu$, it produces a temperature-dependent background in $D(T)$ that decreases as temperature decreases, visible only in the $y = 6.998$ samples. For $T < T_\nu$, $D(T)$ increases in similar fashion for all samples (Fig. 4a): the pseudogap clearly has the effect of increasing $D(T)$. If the chains were responsible for this increase, we would expect it to be largest in the samples with the most highly conducting chains, namely the $y = 6.998$ samples. However, the opposite is true: below T_ν, $D(T)$ is smallest for those samples (Supplementary Fig. 9b). We conclude that chain conduction is not the cause of the pseudogap-related anisotropy in the Nernst coefficient.

This implies that the pseudogap phase breaks the four-fold rotational symmetry of the CuO_2 planes. The orthorhombic distortion of the CuO_2 planes caused by the CuO chains already breaks four-fold symmetry, and this 'weak' symmetry breaking is necessary for any breaking of four-fold rotational symmetry to be observable macroscopically. In its absence, any spontaneous order would form domains and the associated in-plane anisotropy would be averaged out to zero over the volume of the sample[12]. The orthorhombic distortion has the same role as an in-plane magnetic field in a ferromagnet or a metal with nematic order[21].

Broken rotational symmetry places a major constraint on the possible states that can be identified with the pseudogap phase. It

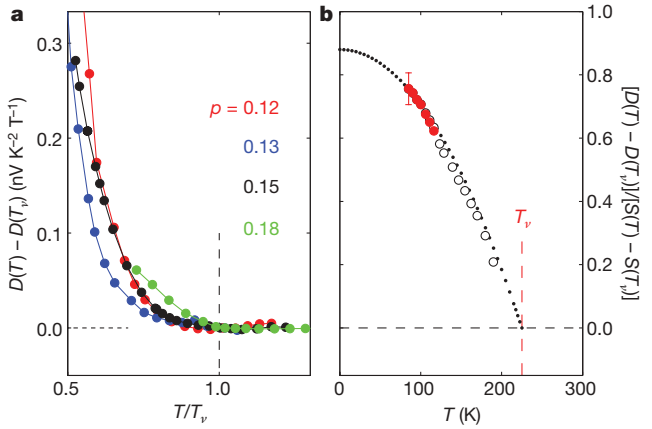

Figure 4 | Anisotropy of the Nernst signal. Difference in the Nernst signal of YBCO between having $\Delta T \,||\, a$ and having $\Delta T \,||\, b$, defined as $D(T) \equiv (\nu_a - \nu_b)/T$. **a**, Difference plotted as $D(T) - D(T_\nu)$ versus T/T_ν for various dopings (as colour-coded; Supplementary Fig. 5 shows the full $D(T)$ data). T_ν is that obtained for the *b*-axis samples (Supplementary Fig. 1 and Supplementary Table 1). The onset of the pseudogap phase, at T_ν, causes a fairly uniform rise in the anisotropy. **b**, Difference plotted as $[D(T) - D(T_\nu)]/[S(T) - S(T_\nu)]$ versus T for $p = 0.12$ (open black circles), where $S(T) \equiv -(\nu_a + \nu_b)/T$. The plotted ratio equals $(\nu_b - \nu_a)/(\nu_b + \nu_a)$ (filled red circles) at low temperature, when $D(T) \gg |D(T_\nu)|$ and $S(T) \gg |S(T_\nu)|$. This ratio can be viewed as a nematic-order parameter (ref. 21). (We note that because $(\nu_b - \nu_a)$ changes sign near 150 K, it is meaningless to plot $(\nu_b - \nu_a)/(\nu_b + \nu_a)$ beyond 120 K or so; see Supplementary Fig. 7.) The error bar on the absolute value of $(\nu_b - \nu_a)/(\nu_b + \nu_a)$ (shown at 90 K) comes from the separate uncertainties of ±10% in ν_b and ν_a (Supplementary Information). The dotted line shows a simple parabolic temperature dependence.

favours 'stripe-like' order, that is, unidirectional modulations of the spin and/or charge density, or nematic order[11,12]. Recent calculations performed for copper oxides confirm that stripe order can cause a major enhancement of the quasiparticle Nernst signal, with a sign that depends on the modulation vector[22], and that nematic order can produce a much larger anisotropy in ν than in σ (ref. 23).

In $La_{2-x}Sr_xCuO_4$ (LSCO) doped with Nd or Eu, the quasiparticle Nernst signal also undergoes an enhancement (and sign change) below a temperature, T_ν, that is equal to T_ρ (ref. 24). Both of these temperatures decrease monotonically with doping in a way that is very similar to the behaviour in YBCO (Fig. 2), with T_ν (and T_ρ) going to zero at a critical doping, $p^* \approx 0.24$ (ref. 25). In these materials, static long-range stripe order has been observed below a temperature, T_{CO}, that decreases with doping and vanishes at $p \approx 0.25$ (ref. 26), with $T_{CO} \approx T_\nu/2$ (ref. 27). The onset of stripe order causes a reconstruction of the Fermi surface at T_{CO} (ref. 27) that, in Eu-doped LSCO at $p = 0.125$, is manifest as a decrease in the Hall coefficient, $R_H(T)$, and the Seebeck coefficient, $S(T)$, to negative values[27,28], starting at $T_{CO} \approx 80$ K. In YBCO at $p = 0.12$, the same drop is observed in both $R_H(T)$ and $S(T)$, at the same temperature[27,28]. The fact that R_H and S/T have large negative values in the normal state at low temperature is ascribed to the formation of an electron pocket in the Fermi surface of YBCO (refs 28, 29). All this argues strongly for stripe-like order in YBCO at low temperature (in the absence of superconductivity).

It therefore seems that the transformation of the electronic state in underdoped copper oxides on cooling proceeds in two stages: a first transformation at T^*, where rotational symmetry is broken, and a second transformation at $T \approx T^*/2$, where translational symmetry is broken (at least in the absence of superconductivity). The first regime may simply be a short-range or fluctuating precursor of the state at low temperature. This two-stage evolution is consistent with neutron scattering studies[8] of YBCO at low doping ($T_c = 35$ K, $p \approx 0.07$). On cooling from high temperature, an anisotropy in the spin fluctuation spectrum appears below 150 K or so, in the form of an incommensurability with the lattice that grows as temperature decreases and is observed along the *a* axis but not the *b* axis[8]. At low temperature, static spin-density-wave order is seen[8]. Although these particular observations are at a doping level below the range of our investigations, the two-stage ordering sequence they reveal at $p \approx 0.07$, namely anisotropic spin fluctuations followed by spin-density-wave order, is consistent with the two-stage process of symmetry breaking revealed by transport measurements at $p = 0.12$. (We note that the in-plane anisotropy of the spin fluctuation spectrum is present up to a doping of at least $p \approx 0.11$ (refs 6, 7).) This type of ordering sequence, that is, fluctuating stripes followed by static stripe order, has been proposed theoretically in the context of a doped Mott insulator[30].

Received 17 September; accepted 25 November 2009.

1. Norman, M. R., Pines, D. & Kallin, C. The pseudogap: friend or foe of high T_c? *Adv. Phys.* **54,** 715–733 (2005).
2. Fauqué, B. *et al.* Magnetic order in the pseudogap phase of high-T_c superconductors. *Phys. Rev. Lett.* **96,** 197001 (2006).
3. Li, Y. *et al.* Unusual magnetic order in the pseudogap region of the superconductor $HgBa_2CuO_{4+\delta}$. *Nature* **455,** 372–375 (2008).
4. Xia, J. *et al.* Polar Kerr effect of the high-temperature superconductor $YBa_2Cu_3O_{6+x}$: evidence of broken symmetry near the pseudogap temperature. *Phys. Rev. Lett.* **100,** 127002 (2008).
5. Ando, Y. *et al.* Electrical resistivity anisotropy from self-organized one dimensionality in high-temperature superconductors. *Phys. Rev. Lett.* **88,** 137005 (2002).
6. Stock, C. *et al.* Dynamical stripes and resonance in the superconducting and normal phases of $YBa_2Cu_3O_{6.5}$ ortho-II superconductor. *Phys. Rev. B* **69,** 014502 (2004).
7. Hinkov, V. *et al.* Spin dynamics in the pseudogap state of a high-temperature superconductor. *Nature Phys.* **3,** 780–785 (2007).
8. Hinkov, V. *et al.* Electronic liquid crystal state in the high-temperature superconductor $YBa_2Cu_3O_{6.45}$. *Science* **319,** 597–600 (2008).
9. Kohsaka, Y. *et al.* An intrinsic bond-centered electronic glass with unidirectional domains in underdoped cuprates. *Science* **315,** 1380–1385 (2007).
10. Kohsaka, Y. *et al.* How Cooper pairs vanish approaching the Mott insulator in $Bi_2Sr_2CaCu_2O_{8+\delta}$. *Nature* **454,** 1072–1078 (2008).
11. Kivelson, S. A. *et al.* How to detect fluctuating stripes in the high-temperature superconductors. *Rev. Mod. Phys.* **75,** 1201–1241 (2003).
12. Vojta, M. Lattice-symmetry breaking in cuprate superconductors: stripes, nematics and superconductivity. *Adv. Phys.* **58,** 699–820 (2009).
13. Liang, R., Bonn, D. A. & Hardy, W. N. Evaluation of CuO_2 plane hole doping in $YBa_2Cu_3O_{6+x}$ single crystals. *Phys. Rev. B* **73,** 180505 (2006).
14. Wang, Y., Li, P. & Ong, N. P. Nernst effect in high-T_c superconductors. *Phys. Rev. B* **73,** 024510 (2006).
15. Rullier-Albenque, F. *et al.* Nernst effect and disorder in the normal state of high-T_c cuprates. *Phys. Rev. Lett.* **96,** 067002 (2006).
16. Ong, N. P. *et al.* Vorticity and the Nernst effect in cuprate superconductors. *Ann. Phys. (Leipz.)* **13,** 9–14 (2004).
17. Behnia, K. The Nernst effect and the boundaries of the Fermi liquid picture. *J. Phys. Condens. Matter* **21,** 113101 (2009).
18. Timusk, T. & Statt, B. The pseudogap in high-temperature superconductors: an experimental survey. *Rep. Prog. Phys.* **62,** 61–122 (1999).
19. Ando, Y. *et al.* Electronic phase diagram of high-T_c cuprate superconductors from a mapping of the in-plane resistivity curvature. *Phys. Rev. Lett.* **93,** 267001 (2004).
20. Matusiak, M. *et al.* Influence of the pseudogap on the Nernst coefficient of $Y_{0.9}Ca_{0.1}Ba_2Cu_3O_y$. *Europhys. Lett.* **86,** 17005 (2009).
21. Borzi, R. A. *et al.* Formation of a nematic fluid at high fields in $Sr_3Ru_2O_7$. *Science* **315,** 214–217 (2007).
22. Hackl, A., Vojta, M. & Sachdev, S. Quasiparticle Nernst effect in stripe-ordered cuprates. Preprint at ⟨http://arXiv.org/abs/0908.1088⟩ (2009).
23. Hackl, A. & Vojta, M. Nernst effect anisotropy as a sensitive probe of Fermi surface distortions from electron-nematic order. Preprint at ⟨http://arXiv.org/abs/0909.4534v2⟩ (2009).
24. Cyr-Choinière, O. *et al.* Enhancement of the Nernst effect by stripe order in a high-T_c superconductor. *Nature* **458,** 743–745 (2009).
25. Daou, R. *et al.* Linear temperature dependence of the resistivity and change in Fermi surface at the pseudogap critical point of a high-T_c superconductor. *Nature Phys.* **5,** 31–34 (2009).
26. Ichikawa, N. *et al.* Local magnetic order vs superconductivity in a layered cuprate. *Phys. Rev. Lett.* **85,** 1738–1741 (2000).
27. Taillefer, L. Fermi surface reconstruction in high-T_c superconductors. *J. Phys. Condens. Matter* **21,** 164212 (2009).
28. Chang, J. *et al.* Thermo-electric study of Fermi surface reconstruction in $YBa_2Cu_3O_y$. Preprint at ⟨http://arXiv.org/abs/0907.5039⟩ (2009).
29. LeBoeuf, D. *et al.* Electron pockets in the Fermi surface of hole-doped high-T_c superconductors. *Nature* **450,** 533–536 (2007).

30. Kivelson, S. A., Fradkin, E. & Emery, V. J. Electronic liquid-crystal phases of a doped Mott insulator. *Nature* **393,** 550–553 (1998).

Supplementary Information is linked to the online version of the paper at www.nature.com/nature.

Acknowledgements We thank K. Behnia, R. L. Greene, C. Kallin, S. A. Kivelson, A. J. Millis, C. Proust, S. Sachdev, A.-M. S. Tremblay and M. Vojta for discussions, and J. Corbin for his assistance with the experiments. J.C. was supported by fellowships from the Swiss National Science Foundation and the Fonds québécois de la recherche sur la nature et les technologies (FQRNT). L.T. acknowledges support from the Canadian Institute for Advanced Research and funding from the Canadian Natural Sciences and Engineering Research Council, the FQRNT, the Canada Foundation for Innovation and a Canada Research Chair.

Author Contributions R.D., J.C., D.L., O.C.-C., F.L. and N.D.-L. performed the Nernst and resistivity measurements; R.D., J.C. and D.L. analysed the Nernst data; B.J.R., R.L., D.A.B. and W.N.H. prepared the samples at the University of British Columbia (crystal growth, annealing, de-twinning, contacts); and L.T. supervised the project and wrote the manuscript.

Author Information Reprints and permissions information is available at www.nature.com/reprints. The authors declare no competing financial interests. Correspondence and requests for materials should be addressed to L.T. (louis.taillefer@physique.usherbrooke.ca).